

Supplement of Atmos. Chem. Phys., 18, 12241–12256, 2018
<https://doi.org/10.5194/acp-18-12241-2018-supplement>
© Author(s) 2018. This work is distributed under
the Creative Commons Attribution 4.0 License.



Supplement of

Effectiveness of ammonia reduction on control of fine particle nitrate

Hongyu Guo et al.

Correspondence to: Rodney J. Weber (rweber@eas.gatech.edu)

The copyright of individual parts of the supplement might differ from the CC BY 4.0 License.

1. Diurnal profiles of T , RH and pH in Cabauw, the Netherlands

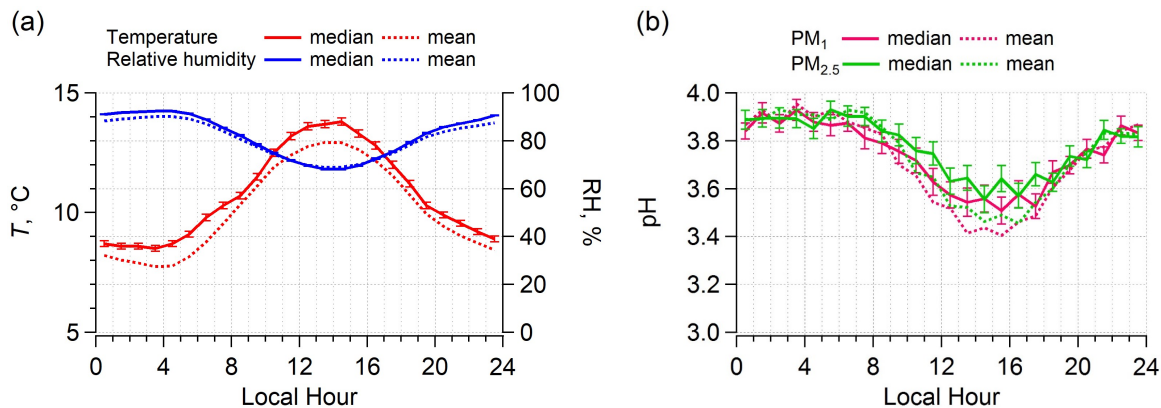


Fig. S1. For the one-year observation at CESAR tower, diurnal profiles of (a) measured T , RH, (b) predicted PM_{10} and $\text{PM}_{2.5}$ pH. Mean hourly medians and means are shown and standard errors are plotted as error bars.

2. Comparison of ideal- and nonideal-condition $\varepsilon(\text{NO}_3^-)$ S curves in Cabauw, the Netherlands

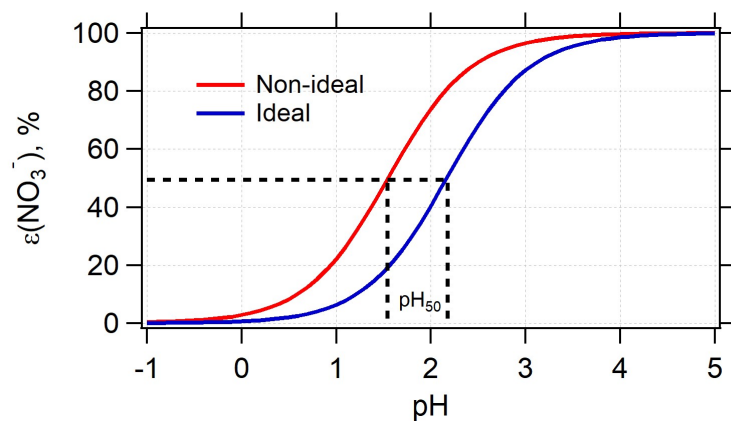


Fig. S2. Predicted particle phase fraction of total nitrate, $\varepsilon(\text{NO}_3^-)$, versus pH for 1-year average condition in Cabauw based on Eq. (4) in the main text. The red and blue lines are based on $\gamma_{\text{NO}_3^-}\gamma_{\text{H}^+} = 0.24$ (extracted from ISORROPIA-II) and 1 (ideal solution), respectively.

3. The thermodynamic model and comparison of predicted and measured gas-particle partitioning in Cabauw, the Netherlands

pH of PM₁ or PM_{2.5} was determined from running the Windows stand-alone executable version of ISORROPIA-II (http://isorropia.eas.gatech.edu/index.php?title=Main_Page) in forward and metastable modes. The model has been proven to accurately predict gas-aerosol partitioning of inorganic species in many studies (Fountoukis and Nenes, 2007; Guo et al., 2016; Guo et al., 2017a; Liu et al., 2017), including particle liquid water (Guo et al., 2015; Bougiatioti et al., 2016). ISORROPIA-II has been used to predict particle pH in several studies (Guo et al., 2015; Hennigan et al., 2015; Guo et al., 2016; Guo et al., 2017a; Liu et al., 2017). pH is a logarithmic scale of hydronium ion activity in an aqueous solution,

$$\text{pH} = -\log_{10} \gamma_{\text{H}^+} H_{\text{aq}}^+ = -\log_{10} \frac{1000 \gamma_{\text{H}^+} H_{\text{air}}^+}{W_i + W_o} \cong -\log_{10} \frac{1000 \gamma_{\text{H}^+} H_{\text{air}}^+}{W_i} \quad (1)$$

where γ_{H^+} is the hydronium ion activity coefficient. γ_{H^+} is assumed = 1, however, ISORROPIA-II calculates the activity coefficients of ionic pairs, such as $\text{H}^+ - \text{NO}_3^-$, so the nonideality effect of H^+ is considered), H_{aq}^+ (mol L⁻¹) is the hydronium ion concentration in particle liquid water, H_{air}^+ (μg m⁻³) is the hydronium ion concentration per volume of air, and W_i , W_o (μg m⁻³) are particle water concentrations associated with inorganic and organic species, respectively. pH predicted solely with W_i is fairly accurate; pH was 0.15-0.23 units systematically lower than and highly correlated to ($r^2 = 0.97$) pH predicted with total particle water ($W_i + W_o$) in the southeastern US, where W_o was on average 35% of total particle water (Guo et al., 2015). In most other location, including this study, a smaller contribution from W_o is expected based on the smaller organic aerosol mass fraction, 29%, (Schlag et al., 2016) compared to the southeastern US, ~60% (Xu et al., 2015). For this study of Cabauw, we only use W_i for the following pH calculations.

As in past studies (Guo et al., 2015; Guo et al., 2016; Guo et al., 2017a), predicted pH was assessed by comparing measured and model-predicted gas-aerosol partitioning of semi-volatile species, such as $\text{NH}_3 - \text{NH}_4^+$, $\text{HNO}_3 - \text{NO}_3^-$, $\text{HCl} - \text{Cl}^-$, when not completely in the gas or aerosol phase. An accurate pH prediction is important in this study, as the nitrate gas-particle partitioning is pH dependent (Guo et al., 2016).

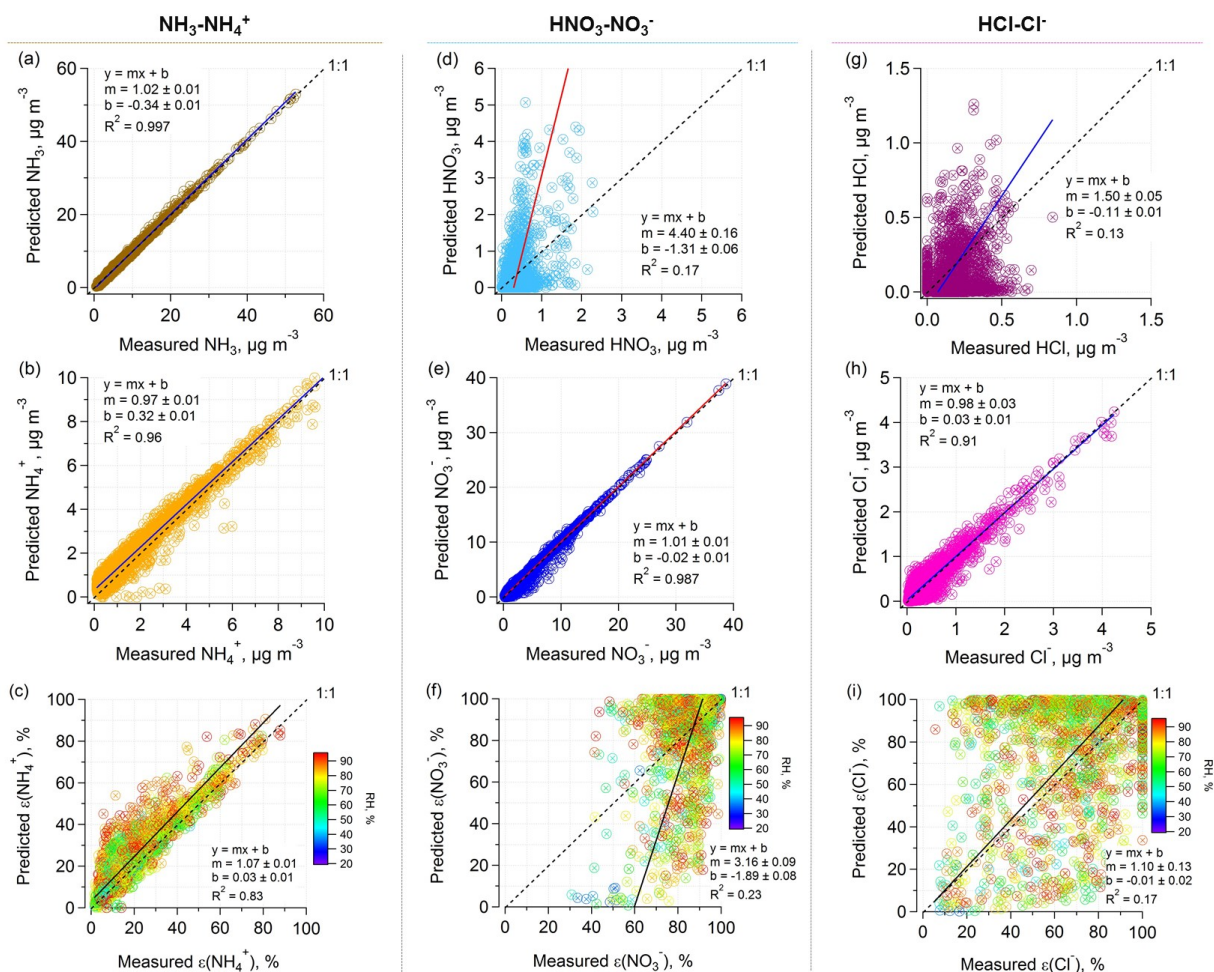


Fig. S3. Comparisons of predicted and measured NH_3 , NH_4^+ , and $\epsilon(\text{NH}_4^+)$ (a, b, c), HNO_3 , NO_3^- , and $\epsilon(\text{NO}_3^-)$ (d, e, f), and HCl , Cl^- , and $\epsilon(\text{Cl}^-)$ (g, h, i) for data from the one-year observational study at CESAR ground site. Gas- and particle-phase ($\text{PM}_{2.5}$) data are all from MARGA. Low concentrations within $2 \times \text{LOD}$ are excluded in plotting particle phase fractions due to high uncertainties. Orthogonal distance regression (ODR) fits are shown and uncertainties in the fits are one standard deviation (SD). Less agreement for gas phase HNO_3 and HCl are thought to be due to significantly lower concentrations than the particle phase component (NO_3^- , Cl^- , respectively). Bias in these gases can be possible if some particles are captured in the denuder, given that the ion chromatographic detection system cannot distinguish between gas and particle phases (NO_3^- and Cl^- is measured for both).

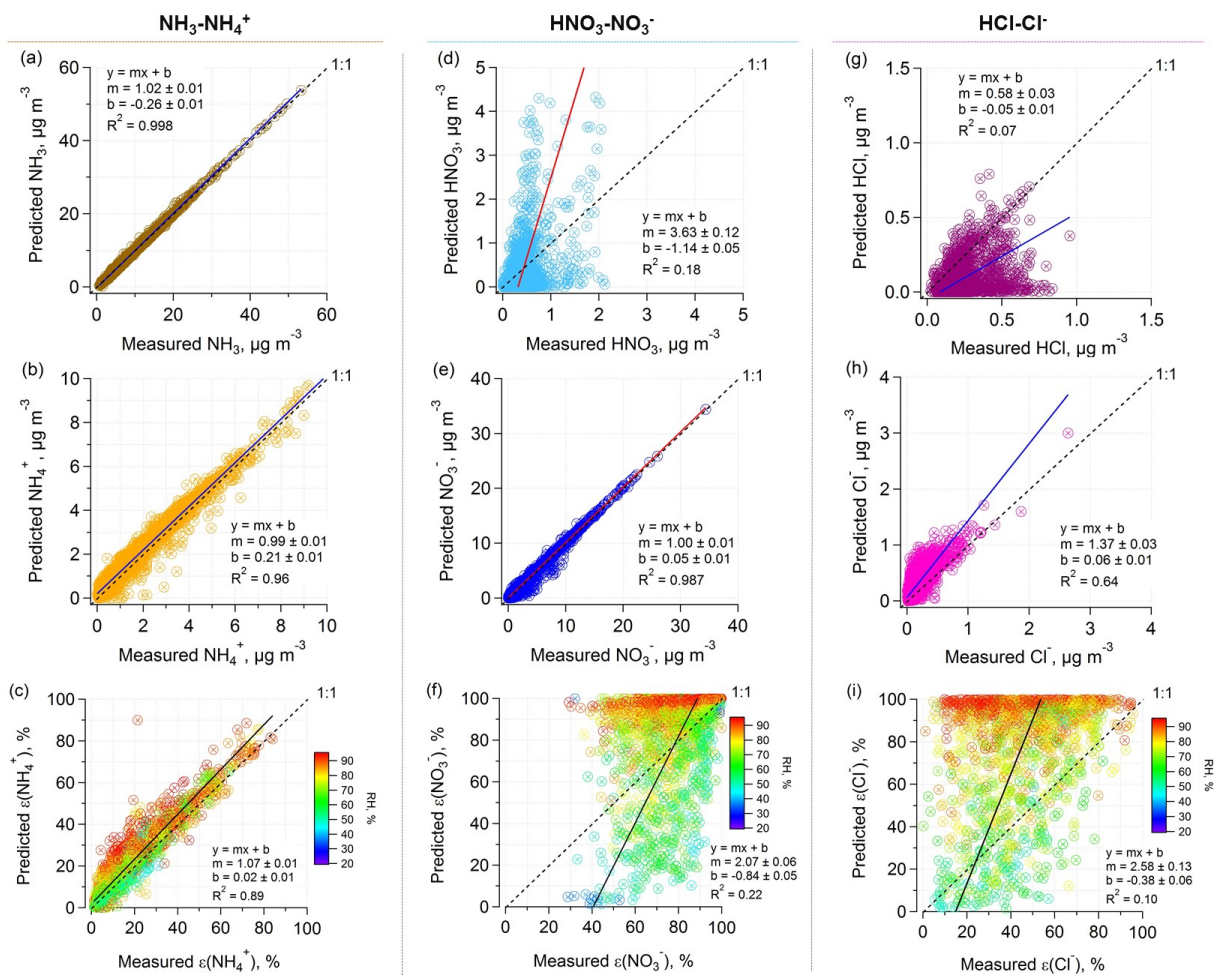


Fig. S4. A similar plot as Fig. S3. MARGA PM₁ data was used in the model input instead of PM_{2.5}.

4. Analytically predicted nitrate partitioning versus pH for various field studies

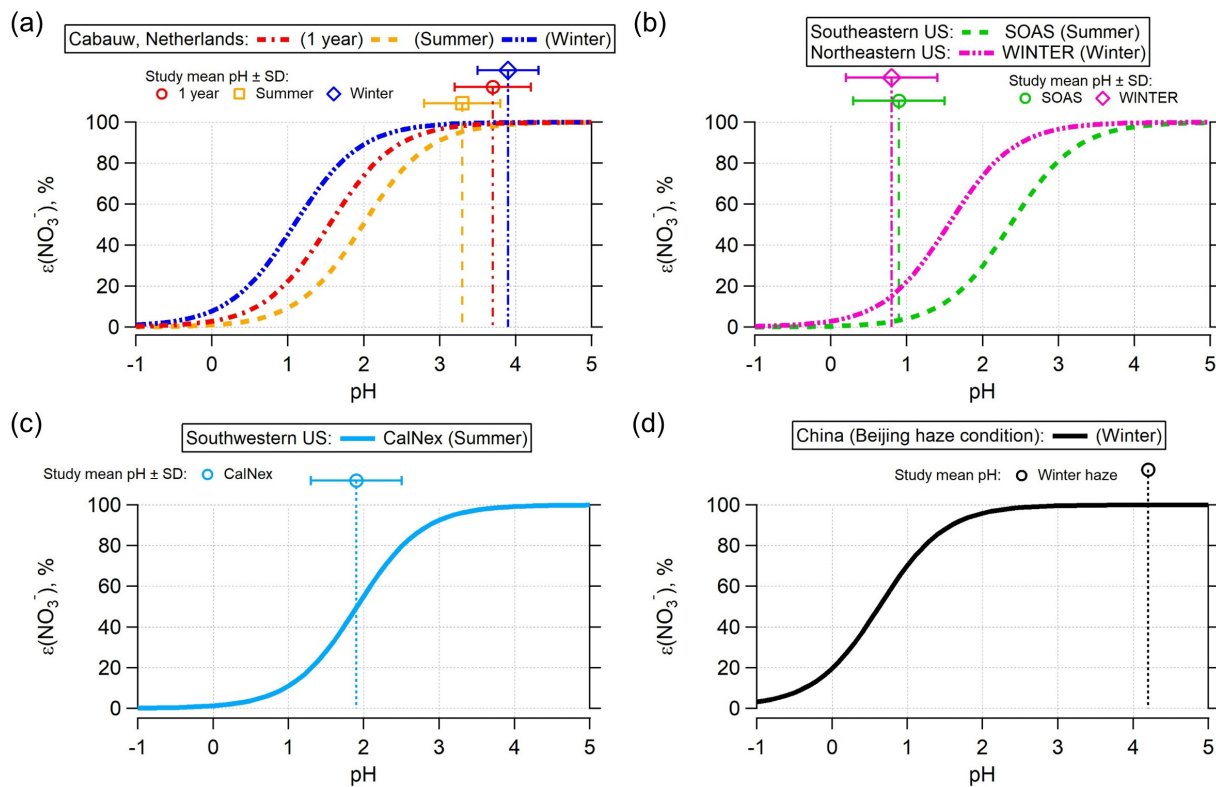


Fig. S5. $\epsilon(\text{NO}_3^-)$ versus pH for the listed field studies. The S curves are calculated based on the average temperature, liquid water, and activity coefficients for each study, according to Eq. (2). The input can be found in Table S1. Vertical lines are the study average ambient fine particle pH calculated with ISORROPIA-II and error bars show the variability in pH as one standard deviation. This figure is reproduced from Figure 2 in the main text, to directly show the seasonal variations at a specific region.

5. Comparison of ISORROPIA-II predicted and analytically predicted pH

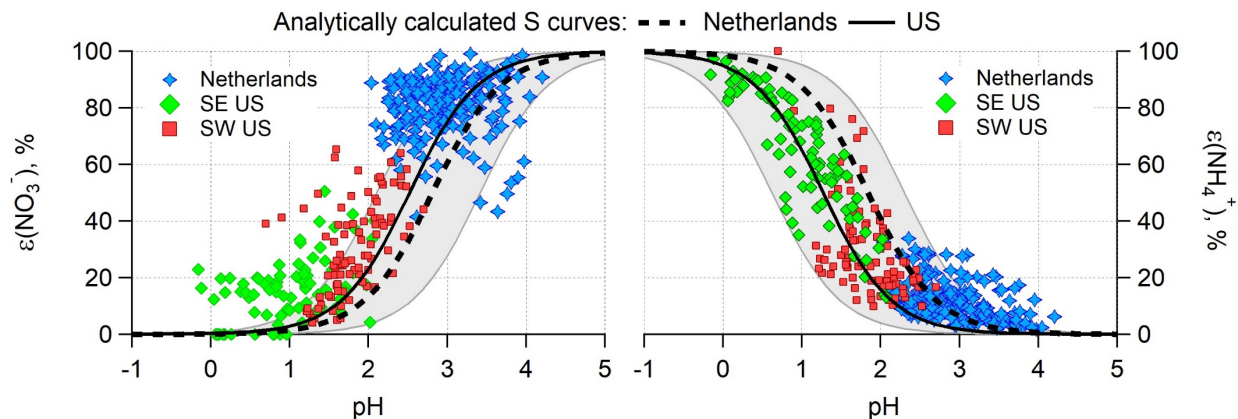


Fig. S6. Analytically calculated S curves of $\epsilon(\text{NO}_3^-)$ and $\epsilon(\text{NH}_4^+)$ (shown as lines), and observed ambient $\epsilon(\text{NO}_3^-)$ and $\epsilon(\text{NH}_4^+)$ plotted with ISORROPIA-predicted pH for SOAS (SE US), CalNex (SW US), and this study at Cabauw (Netherlands) (shown as data points). $\epsilon(\text{NO}_3^-)$ and $\epsilon(\text{NH}_4^+)$ are the particle fraction of gas plus particle for nitrate and ammonium, respectively. The analytical calculations are based on simple thermodynamic equations that can be found in the main text, Eq. (2) for $\epsilon(\text{NO}_3^-)$ or in Guo et al. (2017a) and are independent of ISORROPIA-II calculations. Plotted data are for a relatively narrow range in W_i (1 to $4 \mu\text{g m}^{-3}$) and T (15 to $25 \text{ }^\circ\text{C}$) for comparison with the analytical calculation based on $W_i = 2.5 \mu\text{g m}^{-3}$ and $T = 20 \text{ }^\circ\text{C}$. For the analytical calculations (the black solid and dashed S curves), ISORROPIA-II predicted activity coefficients are applied. For the selected water and temperature ranges, $\gamma_{H^+}\gamma_{\text{NO}_3^-}$ is 0.17 ± 0.10 for Cabauw, 0.086 ± 0.060 for SE US, and 0.087 ± 0.027 for SW US and $\gamma_{H^+}/\gamma_{\text{NH}_4^+}$ is 5.93 ± 6.48 for Cabauw, 1.17 ± 0.12 for SE US, and 1.90 ± 0.12 for SW US. Since the activity coefficients for the US studies are similar, they were averaged to produce one curve for SE US and SW US. Averaged $\gamma_{H^+}/\gamma_{\text{NH}_4^+} = 1.6$ and $\gamma_{H^+}\gamma_{\text{NO}_3^-} = 0.087$. Some of the data scatter can be attributed to variations in liquid water, temperature, and activity coefficients. These effects are illustrated by the light gray shaded regions, which were plotted with different W_i , T , and $\gamma_{H^+}\gamma_{\text{NO}_3^-}$ or $\gamma_{H^+}/\gamma_{\text{NH}_4^+}$. For example, the upper line for $\epsilon(\text{NO}_3^-)$ is calculated using $W_i = 4 \mu\text{g m}^{-3}$, $T = 15 \text{ }^\circ\text{C}$, and $\gamma_{H^+}\gamma_{\text{NO}_3^-} = 0.087$, while the lower line is calculated using $W_i = 1 \mu\text{g m}^{-3}$, $T = 25 \text{ }^\circ\text{C}$, and $\gamma_{H^+}\gamma_{\text{NO}_3^-} = 0.17$. For $\epsilon(\text{NH}_4^+)$, the upper line for is calculated using $W_i = 4 \mu\text{g m}^{-3}$, $T = 15 \text{ }^\circ\text{C}$, and $\gamma_{H^+}/\gamma_{\text{NH}_4^+} = 5.93$, while the lower line is calculated using $W_i = 1 \mu\text{g m}^{-3}$, $T = 25 \text{ }^\circ\text{C}$, and $\gamma_{H^+}/\gamma_{\text{NH}_4^+} = 1.6$.

6. Temperature dependencies of NH₃ and HNO₃ gas-particle partitioning

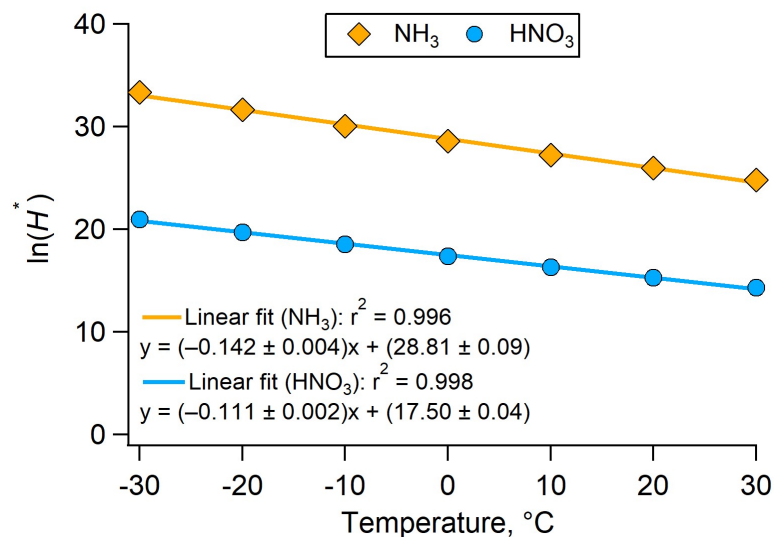


Fig. S7. Molality-based equilibrium constants (H^*) of NH₃-NH₄⁺ and HNO₃-NO₃⁻ partitioning as a function of temperature. $H_{NH_3}^*$ (atm⁻¹) is for NH_{3(g)}+H⁺ ↔ NH₄⁺ and $H_{HNO_3}^*$ (mole² kg⁻² atm⁻¹) is for HNO_{3(g)} ↔ NO₃⁻ + H⁺. The $H_{NH_3}^*$ and $H_{HNO_3}^*$ are calculated based on Clegg et al. (1998) and Clegg and Brimblecombe (1990), respectively, with a typo correction for the equation of $H_{NH_3}^*$. The correction and some instructions to calculate H^* can be found in the supplemental material of Guo et al. (2017a). $H_{NH_3}^*$ decreases faster with increasing temperature compared to $H_{HNO_3}^*$ (slope: -0.142 vs. -0.111), resulting in a net increase in particle H⁺.

7. Particle nitrate and total inorganic mass reduction simulations at less sulfate or more nonvolatile cations condition

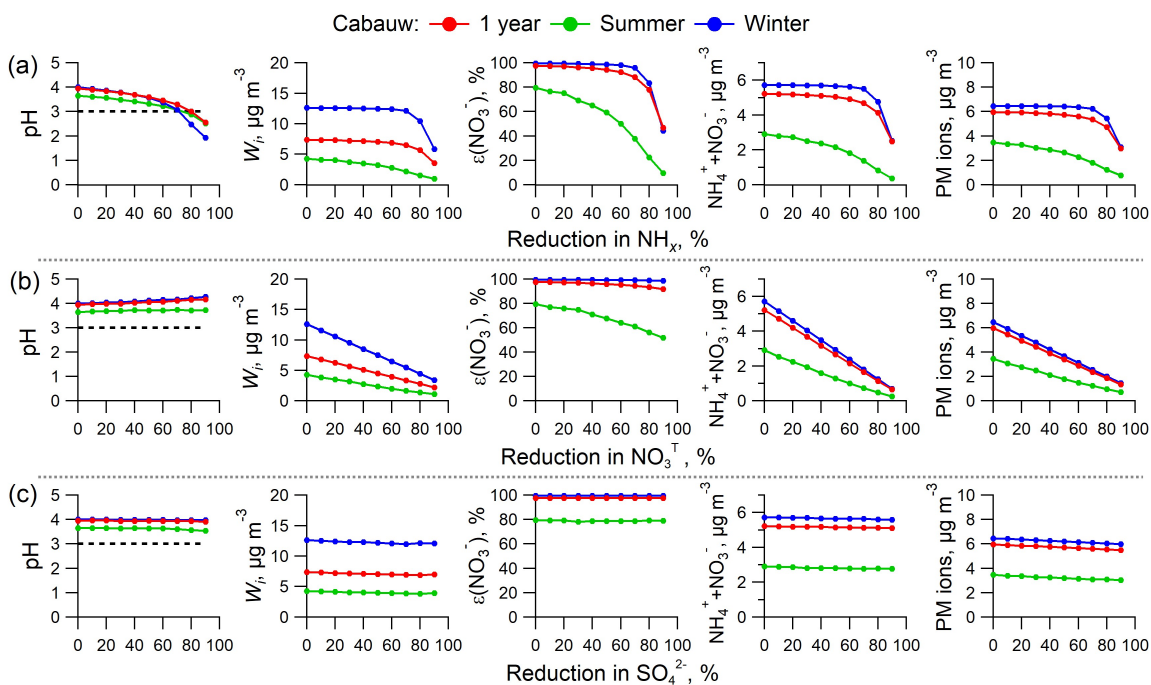


Fig. S8. Similar graph to Figure 4 in the main text, but for simulations with sulfate at 20% of the observed sulfate level while keeping all other inputs unchanged. The prediction of particle pH (first column), liquid water content (W_i , second column), nitrate particle-phase fraction ($\epsilon(\text{NO}_3^-)$, third column), ammonium and nitrate (fourth column), and total aerosol inorganic mass concentrations (fifth column) for reduction of NH_x ($\text{NH}_4^+ + \text{NH}_3$, first row), NO_3^{T} ($\text{NO}_3^- + \text{HNO}_3$, second row), and SO_4^{2-} (third row) with the base case the average conditions of one-year (July 2012-June 2013), summer (June-Aug 2012), and winter (Dec 2012-Feb 2013) observational data in Cabauw, the Netherlands. The black dash lines in the pH figures identifies the critical pH value of 3.

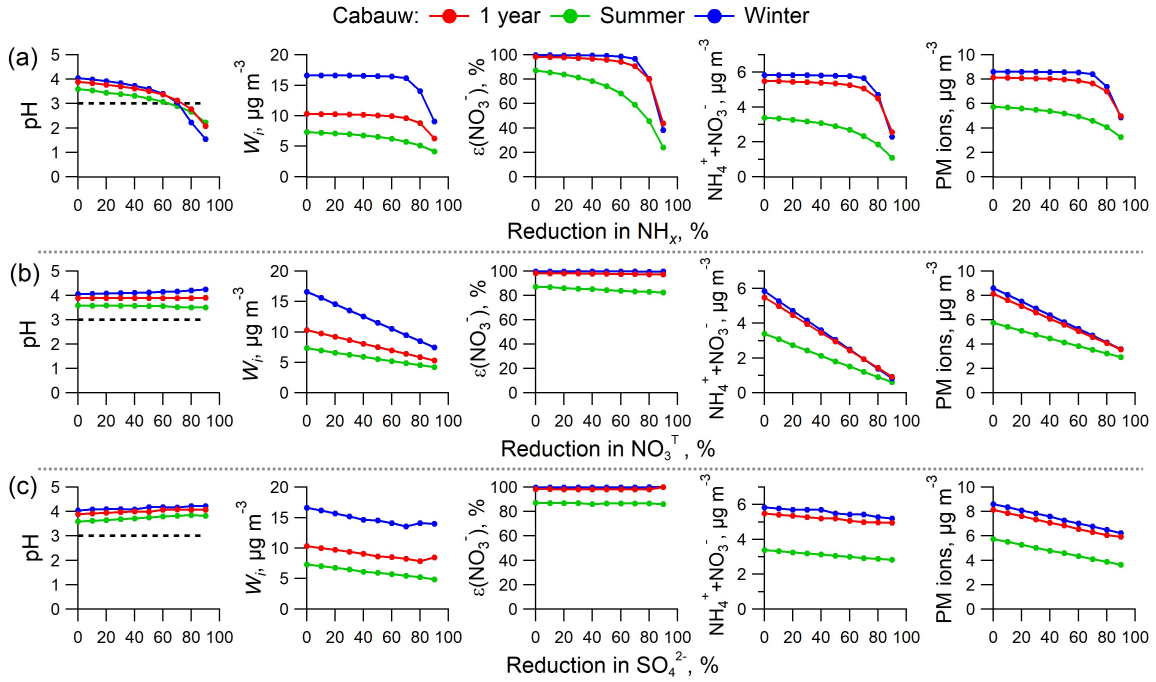


Fig. S9. A similar graph to Figure 4 in the main text and Fig. S8 in the supplement. The above figure shows results with five times of the observed nonvolatile cation levels, while keeping other inputs unchanged. The black dash lines in the pH figures identifies the critical pH value of 3.

8. Summary of thermodynamic modeling inputs and outputs based on the observational averages in Cabauw, the Netherlands, and previously published observational averages at several other sites.

Table. S1. Study average aerosol composition and meteorological conditions for various sites. Various concentrations, RH, and T are based on field measurements, unless noted specifically.

(Region) Country	SE US	NE US	SW US	Netherlands			China
Site location	Centreville, AL	Hampton, VA	Pasadena, CA	Cabauw			Beijing
Campaign	SOAS	WINTER	CalNex	EU-FP7-ACTRIS (Q-ACSM Network)			\
Sampling type	Ground	Aircraft	Ground	Ground			Ground
PM cut size	PM ₁ &PM _{2.5} ^a	PM ₁	PM ₁ ^c	PM _{2.5}			PM ₁
Year	2013	2015	2010	2012-2013			2013
Season	Summer	Winter	(Early) Summer	One-year	Summer	Winter	Winter
Na ⁺ , μg m ⁻³	0.03	0	0	0.14	0.17	0.15	0
SO ₄ ²⁻ , μg m ⁻³	1.73	1.02	2.86	2.20	1.86	2.51	26
NH ₄ ⁺ +NH ₃ , μg m ⁻³	0.78	0.50	3.44	9.63	11.44	6.73	32.8
NO ₃ ⁻ +HNO ₃ , μg m ⁻³	0.45	2.21	10.22	4.87	3.48	5.50	26
Cl ⁻ +HCl, μg m ⁻³	0.02	0	0	0.53	0.44	0.54	1.7
Ca ²⁺ , μg m ⁻³	0	0	0	0.01	0.02	0.001	0
K ⁺ , μg m ⁻³	0	0	0	0.004	0.01	0.002	0
Mg ²⁺ , μg m ⁻³	0	0	0	0.03	0.01	0.04	0
RH, %	74	58	79	78	78	85	56
T , °C	24.7	-0.4	18.3	9.0	17.8	2.4	0.9
NH ₄ ⁺ , μg m ⁻³	0.46	0.50	2.06	1.90	1.51	2.13	20
NH ₃ , μg m ⁻³	0.39	0.10 ^b	1.37	7.73	9.94	4.60	12.8
ϵ (NH ₄ ⁺), %	59	91 ^b	56	19	14	27	60
NO ₃ ⁻ , μg m ⁻³	0.08	0.80	3.58	4.53	3.08	5.28	26
HNO ₃ , μg m ⁻³	0.36	1.41	6.65	0.35	0.40	0.22	\
ϵ (NO ₃ ⁻), %	22	39	39	88	84	91	\
HCl, μg m ⁻³	\	\	\	0.13	0.16	0.03	\
Cl ⁻ , μg m ⁻³	0.02	0	0	0.40	0.28	0.51	1.7
ϵ (Cl ⁻), %	\	\	\	66	52	89	\
$\gamma_{NO_3^-} \gamma_{H^+}$	0.08	0.06	0.14	0.24	0.20	0.24	0.11 ^d
Liquid water, μg m ⁻³	5.1	2.0	13.9	21.7	15.7	31.4	35.1 ^d
$\Delta pH / \Delta(\log_{10} NH_3)$	1.01	1.03	1.07	1.05	1.16	1.00	1.00 ^d
pH	0.9 ± 0.6	0.8 ± 1.0	1.9 ± 0.5	3.7 ± 0.5	3.3 ± 0.5	3.9 ± 0.4	4.2 ^d
Reference	(Guo et al., 2015)	(Guo et al., 2016)	(Guo et al., 2017a)	This study			(Wang et al., 2016)

ISORROPIA-II input

Input related parameters

ISORROPIA-II output

^a PM_{2.5} was sampled in the 1st half and PM₁ sampled in the 2nd half of the study; various parameters were similar in both cases, crustal components were higher in PM_{2.5}, but generally low so differences had minor effects, e.g., PM_{2.5} Na⁺ was 0.06 ± 0.09 μg m⁻³ and PM₁ Na⁺ was 0.01 ± 0.01 μg m⁻³; ^b Prediction based on iteration; ^c PM_{2.5} data was only available for the last week, so here we focus on PM₁ collected throughout the campaign; ^d The model results are from another publication, Guo et al. (2017b).

References

- Bougiatioti, A., Nikolaou, P., Stavroulas, I., Kouvarakis, G., Weber, R., Nenes, A., Kanakidou, M., and Mihalopoulos, N.: Particle water and pH in the Eastern Mediterranean: Sources variability and implications for nutrients availability, *Atmos. Chem. Phys.*, 16, 4579-4591, doi: 10.5194/acp-16-4579-2016, 2016.
- Clegg, S. L., and Brimblecombe, P.: Equilibrium partial pressures and mean activity and osmotic coefficients of 0-100% nitric acid as a function of temperature, *Journal of Physical Chemistry*, 94, 5369-5380, doi: 10.1021/j100376a038, 1990.
- Clegg, S. L., Brimblecombe, P., and Wexler, A. S.: Thermodynamic model of the system H^+ - NH_4^+ - SO_4^{2-} - NO_3^- - H_2O at tropospheric temperatures, *J. Phys. Chem. A*, 102, 2137-2154, doi: 10.1021/Jp973042r, 1998.
- Fountoukis, C., and Nenes, A.: ISORROPIA II: a computationally efficient thermodynamic equilibrium model for K^+ - Ca^{2+} - Mg^{2+} - NH_4^+ - Na^+ - SO_4^{2-} - NO_3^- - Cl^- - H_2O aerosols, *Atmos. Chem. Phys.*, 7, 4639-4659, doi: 10.5194/acp-7-4639-2007, 2007.
- Guo, H., Xu, L., Bougiatioti, A., Cerully, K. M., Capps, S. L., Hite, J. R., Carlton, A. G., Lee, S. H., Bergin, M. H., Ng, N. L., Nenes, A., and Weber, R. J.: Fine-particle water and pH in the southeastern United States, *Atmos. Chem. Phys.*, 15, 5211-5228, doi: 10.5194/acp-15-5211-2015, 2015.
- Guo, H., Sullivan, A. P., Campuzano-Jost, P., Schroder, J. C., Lopez-Hilfiker, F. D., Dibb, J. E., Jimenez, J. L., Thornton, J. A., Brown, S. S., Nenes, A., and Weber, R. J.: Fine particle pH and the partitioning of nitric acid during winter in the northeastern United States, *J. Geophys. Res.*, 121, 10355-10376, doi: 10.1002/2016jd025311, 2016.
- Guo, H., Liu, J., Froyd, K. D., Roberts, J. M., Veres, P. R., Hayes, P. L., Jimenez, J. L., Nenes, A., and Weber, R. J.: Fine particle pH and gas-particle phase partitioning of inorganic species in Pasadena, California, during the 2010 CalNex campaign, *Atmos. Chem. Phys.*, 17, 5703-5719, doi: 10.5194/acp-17-5703-2017, 2017a.
- Guo, H., Weber, R. J., and Nenes, A.: High levels of ammonia do not raise fine particle pH sufficiently to yield nitrogen oxide-dominated sulfate production, *Sci. Rep.*, 7, doi: 10.1038/s41598-017-11704-0, 2017b.
- Hennigan, C. J., Izumi, J., Sullivan, A. P., Weber, R. J., and Nenes, A.: A critical evaluation of proxy methods used to estimate the acidity of atmospheric particles, *Atmos. Chem. Phys.*, 15, 2775-2790, doi: 10.5194/acp-15-2775-2015, 2015.
- Liu, M., Song, Y., Zhou, T., Xu, Z., Yan, C., Zheng, M., Wu, Z., Hu, M., Wu, Y., and Zhu, T.: Fine particle pH during severe haze episodes in northern China, *Geophys. Res. Lett.*, 44, 5213-5221, doi: 10.1002/2017gl073210, 2017.
- Schlag, P., Kiendler-Scharr, A., Blom, M. J., Canonaco, F., Henzing, J. S., Moerman, M., Prévôt, A. S. H., and Holzinger, R.: Aerosol source apportionment from 1-year measurements at the CESAR tower in Cabauw, the Netherlands, *Atmos. Chem. Phys.*, 16, 8831-8847, doi: 10.5194/acp-16-8831-2016, 2016.
- Wang, G., Zhang, R., Gomez, M. E., Yang, L., Levy Zamora, M., Hu, M., Lin, Y., Peng, J., Guo, S., Meng, J., Li, J., Cheng, C., Hu, T., Ren, Y., Wang, Y., Gao, J., Cao, J., An, Z., Zhou, W., Li, G., Wang, J., Tian, P., Marrero-Ortiz, W., Secrest, J., Du, Z., Zheng, J., Shang, D., Zeng, L., Shao, M., Wang, W., Huang, Y., Wang, Y., Zhu, Y., Li, Y., Hu, J., Pan, B., Cai, L., Cheng, Y., Ji, Y., Zhang, F., Rosenfeld, D., Liss, P. S., Duce, R. A., Kolb, C. E., and Molina, M. J.: Persistent sulfate formation from London Fog to Chinese haze, *Proc. Natl. Acad. Sci. U.S.A.*, 113, 13630-13635, doi: 10.1073/pnas.1616540113, 2016.
- Xu, L., Suresh, S., Guo, H., Weber, R. J., and Ng, N. L.: Aerosol characterization over the southeastern United States using high-resolution aerosol mass spectrometry: spatial and seasonal variation of aerosol composition and sources with a focus on organic nitrates, *Atmos. Chem. Phys.*, 15, 7307-7336, doi: 10.5194/acp-15-7307-2015, 2015.